

Structural properties of the geometrically frustrated pyrochlore $\text{Tb}_2\text{Ti}_2\text{O}_7$

S.-W. Han,^{1,*} J. S. Gardner,^{2,3,†} and C. H. Booth^{1,‡}

¹*Chemical Sciences Division, Lawrence Berkeley National Laboratory, Berkeley, California 94720*

²*NIST Center for Neutron Research, National Institute of Standards and Technology, Gaithersburg, Maryland 20899-8562*

³*Physics Department, Brookhaven National Laboratory, Upton, New York 11973*

(Dated: To appear in Phys. Rev. B, scheduled issue January 1, 2004)

Although materials that exhibit nearest-neighbor-only antiferromagnetic interactions and geometrical frustration theoretically should not magnetically order in the absence of disorder, few such systems have been observed experimentally. One such system appears to be the pyrochlore $\text{Tb}_2\text{Ti}_2\text{O}_7$. However, previous structural studies indicated that $\text{Tb}_2\text{Ti}_2\text{O}_7$ is an imperfect pyrochlore. To clarify the situation, we performed neutron powder diffraction (NPD) and x-ray absorption fine structure (XAFS) measurements on samples that were prepared identically to those that show no magnetic order. The NPD measurements show that the long-range structure of $\text{Tb}_2\text{Ti}_2\text{O}_7$ is well ordered with no structural transitions between 4.5 and 600 K. In particular, mean-squared displacements ($\langle u^2 \rangle$'s) for each site follow a Debye model with no offsets. No evidence for Tb/Ti site interchange was observed within an upper limit of 2%. Likewise, no excess or deficiency in the oxygen stoichiometry was observed, within an upper limit of 2% of the nominal pyrochlore value. Tb L_{III} - and Ti K -edge XAFS measurements from 20-300 K similarly indicate a well-ordered local structure. Other aspects of the structure are considered. We conclude that $\text{Tb}_2\text{Ti}_2\text{O}_7$ has, within experimental error, an ideal, disorder-free pyrochlore lattice, thereby allowing the system to remain in a dynamic, frustrated spin state to the lowest observed temperatures.

PACS numbers: 75.25.+z, 75.40.Gb, 75.50.Ee, 75.50.Lk, 61.12.Ld, 61.10.Ht

I. INTRODUCTION

The term *geometrical frustration*^{1,2,3} indicates when the spins on a well-ordered lattice interact magnetically, yet individual interactions cannot reach their minimum energy configuration because of competing magnetic interactions from other sites. A simple example occurs on a two-dimensional, corner-shared triangular lattice with antiferromagnetic nearest-neighbor coupling, otherwise known as a *kagomé* lattice. The three dimensional analogue to such a lattice is a corner-shared tetrahedral lattice, and is realized in the pyrochlore systems, $A_2B_2O_7$.

Theoretically, it has been shown that Heisenberg, antiferromagnetic nearest-neighbor interacting spin systems⁴ do not possess a transition into an ordered state. This makes corner-sharing tetrahedral spin systems with antiferromagnetic exchange ideal candidates for three-dimensional, low temperature spin-liquids. A spin-liquid state may not form if further interactions such as crystal field anisotropy,⁵ long-range exchange or dipolar interactions perturb the classical spin models.⁶ However, since *any* amount of lattice disorder can precipitate a spin-glass phase,⁷ geometrically-frustrated systems that do not magnetically order to the lowest temperatures are extremely rare.⁸ This situation has inhibited experimental studies that attempt to isolate the effects of frustration. For instance, lattice imperfections in several geometrically frustrated systems are thought to relieve the frustration allowing the system to freeze. Néel order has been observed in the Jarosites, $\text{KCr}_3(\text{OD})_6(\text{SO}_4)_2$, which contains Cr^{3+} , $\text{S}=\frac{3}{2}$ ions on a kagomé lattice,⁹ due to vacancies on the magnetic site. Site disorder in $\text{SrCr}_9\text{Ga}_{12-9p}\text{O}_{19}$,¹⁰ for example, facilitates the for-

mation of a spin glass state, as does intersite mixing in $\text{Gd}_3\text{Ga}_5\text{O}_{12}$.^{11,12}

Significantly, the pyrochlore lattice¹³ appears to be capable of producing a spin-liquid state. The magnetic-oxide pyrochlores have the chemical formula $A_2B_2O(1)_6O(2)$ (space group $Fd\bar{3}m$). Here, we focus on the case where the A site is occupied by a trivalent rare-earth ion with eightfold oxygen coordination, $\text{AO}(2)_2\text{O}(1)_6$, and the B site is occupied by a tetra-valent transition metal ion with sixfold oxygen co-ordination, $\text{BO}(1)_6$. The A and B sites individually form infinite interpenetrating sublattices of corner-sharing tetrahedra. A high degree of magnetic frustration is exhibited on this lattice when either site is occupied by antiferromagnetically coupled ions.

Materials with the $A_2B_2O_7$ formula unit can have various structures, some of which can be thought of as defected versions of the fluorite (CaF_2) unit cell. The cubic fluorite cell has Ca atoms at the center of eight F atoms at the corners of a cube. This cell is analogous to one eighth that of the oxide pyrochlore with a random distribution of the metal cations, one oxygen vacancy (the $8a$ site), and the positional parameter x for the oxygens on the $48f$ site equal to $3/8$. The rare-earth titanate pyrochlores have $x \approx 0.328$.¹⁴ Obviously, these structures are related, but the mixing of the metal ions in the fluorite structure creates multiple exchange constants, usually resulting in a static magnetic structure. Other materials with the stoichiometry $A_2B_2O_7$ include the weberites, which are closely related to the pyrochlore structure, but only half the B -site ions have the sixfold oxygen coordination, while the others are linked through only four vertices.

Despite the inherent geometrical frustration in the ideal pyrochlore lattice, most pyrochlores order magnetically. $\text{Tb}_2\text{Ti}_2\text{O}_7$, on the other hand, appears to be the rare case of a pyrochlore that does not order magnetically, exhibiting a high degree of frustration (the large Tb^{3+} moment has a Curie-Weiss temperature of ~ 19 K) down to 70 mK.^{15,16,17} However, the pyrochlore system is also capable of producing a lattice with fairly subtle disorder that can precipitate a spin-glass phase, such as in the Mo-Mo near-neighbor pairs in $\text{Y}_2\text{Mo}_2\text{O}_7$.^{18,19} A similar mechanism may also precipitate the spin-glass phase in $\text{Tb}_2\text{Mo}_2\text{O}_7$.²⁰ In fact, the lack of such frozen magnetic states in $\text{Tb}_2\text{Ti}_2\text{O}_7$ is somewhat surprising, given the results of previous structural measurements. The crystal structure of $\text{Tb}_2\text{Ti}_2\text{O}_7$ was first investigated by Brixner²¹ in 1964. The most detailed structural study is reported by van de Velde *et al.*²² The International Centre for Diffraction Data quotes van de Velde's data as the standard for $\text{Tb}_2\text{Ti}_2\text{O}_7$. Their x-ray diffraction study finds that the measured $\text{Tb}_2\text{Ti}_2\text{O}_7$ sample has approximately 10% disorder on the metal cation and oxygen sublattices, and the authors conclude that $\text{Tb}_2\text{Ti}_2\text{O}_7$ is an imperfect pyrochlore. The study we report below was motivated by this result and attempts to definitively answer the question of lattice imperfections in $\text{Tb}_2\text{Ti}_2\text{O}_7$, a significant parameter in any model that would successfully describe the magnetic nature of $\text{Tb}_2\text{Ti}_2\text{O}_7$.

The present work reports neutron powder diffraction (NPD) measurements of the average structure, and carefully considers the thermal dependence of the mean-squared displacement parameters as a means of separating the non-Debye (presumably static) component of any positional disorder. In addition, the x-ray absorption fine-structure (XAFS) technique is used to check for disorder in the local environment around Tb and Ti atoms, and in particular for the kind of *B*-site correlated disorder that occurs in $\text{Y}_2\text{Mo}_2\text{O}_7$. Finally, the results from the two techniques are combined to determine to what degree correlations exist between several atom pairs.

The rest of this paper is organized as follows: Sample preparation and experimental details are in Sec. II. Data analysis procedures and results are reported in Sec. III. Consequences of these results, comparisons to previous measurements, and further discussion are in Sec. IV, and the final conclusions are in Sec. V.

II. EXPERIMENTAL DETAILS

Polycrystalline $\text{Tb}_2\text{Ti}_2\text{O}_7$ was prepared by a conventional solid state reaction in the same manner as in Ref. 15, namely, by firing stoichiometric amounts of Tb_4O_7 and TiO_2 at 1350° for several days with intermittent grindings to ensure a complete reaction. The neutron diffraction measurements were performed on the time-of-flight Special Environment Powder Diffractometer at the Intense Pulsed Neutron Source (IPNS) at Argonne National Laboratory and on the C2 diffractometer at the

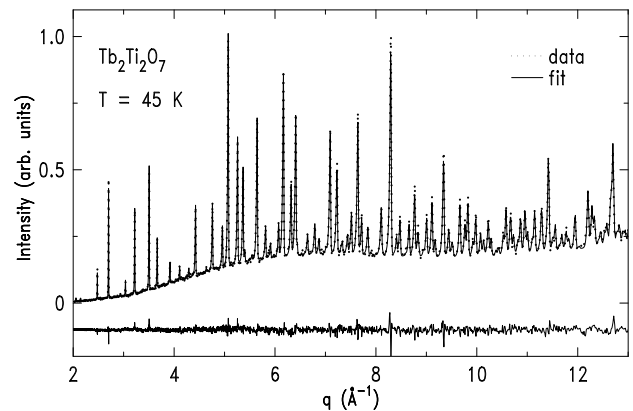


FIG. 1: Neutron diffraction data collected at IPNS from powder $\text{Tb}_2\text{Ti}_2\text{O}_7$ at 45 K as a function of the momentum transfer q . The solid curve is the best fit from the Rietveld refinement with the $Fd\bar{3}m$ structure. The bottom curve shows the difference between the measured and calculated intensities.

NRU reactor at Chalk River Laboratories. The ground powder was packed in a vanadium can and cooled in a displax (IPNS) or a helium-bath cryostat (NRU). A Si(113) crystal was used at the NRU reactor to produce a monochromatic neutron beam with a wavelength of 1.3283 Å. The large difference in the scattering lengths, in particular the negative scattering length of titanium, creates a large contrast with the terbium scattering. This contrast allows for an accurate determination of the crystal structure properties, and especially for any possible cation antisite disorder.

For XAFS measurements, the polycrystalline $\text{Tb}_2\text{Ti}_2\text{O}_7$ sample was re-ground and passed through a 20 μm sieve. The sieved powder was uniformly distributed over adhesive tape, cut into strips and stacked to obtain absorption edge steps of 0.8 absorption lengths at the Ti *K* edge and 1.0 absorption lengths at the Tb *L*_{III} edge. Samples were then placed into a LHe-flow cryostat. Transmission XAFS data were collected at the Stanford Synchrotron Radiation Laboratory (SSRL). Tb *L*_{III}-edge (7515 eV) data were collected on beamline 4-3 with a 1/2-tuned Si(220) double-crystal monochromator. Ti *K*-edge (4965 eV) data were collected on beamline 2-3 with a 1/2-tuned Si(111) double-crystal monochromator.

III. RESULTS

The rare earth oxide pyrochlores crystallize in the space group $Fd\bar{3}m$ as mentioned above, with 4 crystallographically independent sites (A^{3+} in position $16d$ at $(\frac{1}{2}, \frac{1}{2}, \frac{1}{2})$, B^{4+} in $16c$ at $(0, 0, 0)$, O(1) in $48f$ at $(x, \frac{1}{8}, \frac{1}{8})$ and O(2) in $8b$ at $(\frac{3}{8}, \frac{3}{8}, \frac{3}{8})$ ¹³). The position of the $48f$ site is defined by only one variable, x , which is sensitive to lattice effects, including the absolute size and the relative difference in size of the metal ions, as well as to various forms of disorder.²³

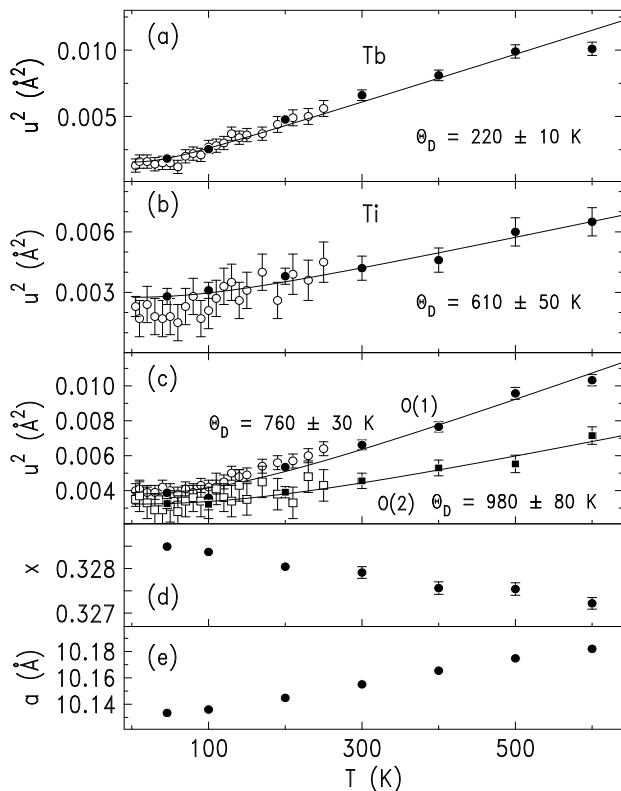


FIG. 2: Mean-squared displacement parameters, u^2 's, for the 4 crystallographic sites of $\text{Tb}_2\text{Ti}_2\text{O}_7$ as a function of temperature are shown in panels (a)-(c). The data were collected at the IPNS (closed symbol) and the NRU reactor (open symbol). Solid lines are best fits using a Debye model (see Table I). Panels (d) and (e) show the temperature dependence of the positional parameter x of the O(1) oxygen (48f site) and the lattice parameter a , respectively.

The neutron diffraction data were analyzed with a Rietveld method using the General Structure Analysis System (GSAS) refinement package.²⁴ Figure 1 shows the 45 K data together with the best refinement and the residual, shown at the bottom. No additional peaks, associated with either a second phase or a magnetic unit cell, were observed over the whole temperature range from 4.5-600 K. However as previously reported,¹⁵ an anomalous background due to short range magnetic correlations was observed at the lowest temperatures. The atomic displacement parameters of all atoms were assumed to be isotropic during the fitting process since no improvement in the refinement was obtained by using anisotropic parameters. This is in contrast to $\text{Y}_2\text{Mo}_2\text{O}_7$, where anisotropic parameters for the A site were deemed necessary.²⁵ The results of the refinement are summarized in Table I. The possibility of antisite disorder (site interchange between Tb and Ti atoms) was also considered, such as could occur if the system had a propensity toward a fluorite-like structure.^{26,27} We find no evidence for any such disorder, and place an upper limit of 2% on metal-site mixing. Similarly, we performed fits al-

TABLE I: NPD fit results to IPNS data from $\text{Tb}_2\text{Ti}_2\text{O}_7$ using the $Fd\bar{3}m$ space group. Reported values are from fits at 45 K, except for the Debye fit results, which are over the full temperature range of the data (45 - 600 K). Static disorders were obtained with the Debye model fit shown in Fig. 2. All site occupancies are fixed at unity.

| General fit characteristics: | | | | | | |
|------------------------------|-------------------------------|-----|-----|----------------------------------|----------------|-------------------------------------|
| Banks included | $\pm 145^\circ, \pm 90^\circ$ | | | | | |
| Total data points | 8792 | | | | | |
| Total measured reflections | 362 | | | | | |
| # of variables | 9+4 for background | | | | | |
| reduced χ^2 | 1.802 | | | | | |
| $Rp(\%)$ | 6.90 | | | | | |
| $wRp(\%)$ | 4.51 | | | | | |
| Atom | x | y | z | $u_{\text{iso}}^2(\text{\AA}^2)$ | Θ_D (K) | $u_{\text{static}}^2(\text{\AA}^2)$ |
| Tb | 1/2 | 1/2 | 1/2 | 0.0018(2) | 220(10) | 0.0006(7) |
| Ti | 0 | 0 | 0 | 0.0028(4) | 610(50) | 0.0015(12) |
| O(1) | 0.3285(1) | 1/8 | 1/8 | 0.0039(2) | 760(30) | 0.0010(12) |
| O(2) | 3/8 | 3/8 | 3/8 | 0.0033(3) | 980(80) | 0.0008(12) |
| a_0 | 10.13315(12) \AA | | | | | |
| Tb-O(2)-Tb | 109.47(1) $^\circ$ | | | | | |
| Tb-O(1)-Tb | 106.41(3) $^\circ$ | | | | | |
| Tb-O(1)-Ti | 106.41(2) $^\circ$ | | | | | |
| Ti-O(1)-Ti | 132.12(5) $^\circ$ | | | | | |

lowing the oxygen occupancy fractions to vary, including the possibility of oxygen on the nominally vacant $8a$ site. These measurements provide no evidence of excess or deficient oxygen compared to the nominal pyrochlore structure within an upper limit of 2%. Both of these limits are considerably lower than the disorder reported by van de Velde *et al.*²²

Figure 2 shows the mean-squared displacements, u^2 , for all four crystallographic sites and the positional parameter, x , as a function of temperature. No structural anomalies, within uncertainty, were observed. The u^2 's for each site were fit with a thermal model, including a temperature-independent offset:

$$u_{\text{meas}}^2(T) = u_{\text{static}}^2 + u_{\text{thermal}}^2(T). \quad (1)$$

The temperature-dependent part of the mean-squared displacement parameters, $u_{\text{thermal}}^2(T)$, is given in general by a collection of quantum harmonic oscillators:

$$u_{\text{thermal}}^2(T) = \frac{\hbar}{2m} \int_0^\infty \rho(\omega) \coth\left(\frac{\hbar\omega}{2k_B T}\right) \frac{d\omega}{\omega} \quad (2)$$

where m is the atomic mass and ρ is the phonon density of states at the given site. In the Debye model, the density of states is empty above a cutoff frequency, ω_D , and quadratic below it: $\rho = 3\omega^2/\omega_D^3$. The Debye temperature is then just $\theta_D = \hbar\omega_D/k_B$. Note that zero-point motion exists such that even in the absence of a static

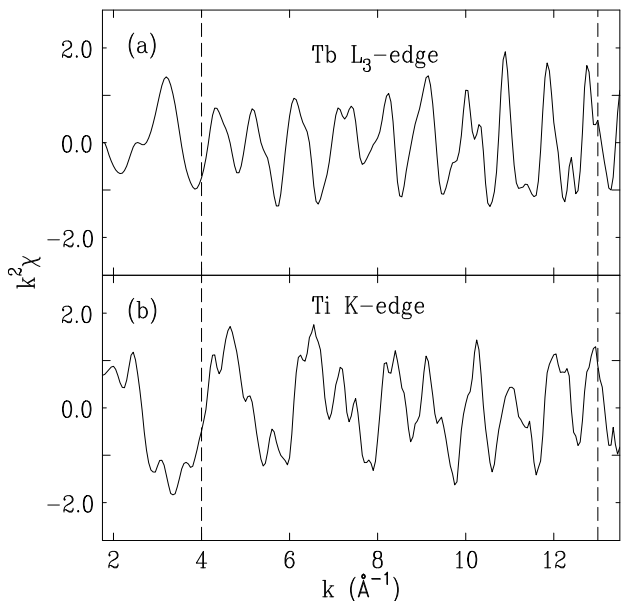


FIG. 3: XAFS data at 20 K measured above the (a) Tb L_3 -edge and (b) Ti K -edge as a function of photoelectron wave number, k .

offset, μ_{thermal}^2 is not zero at $T=0$, and is, in fact:

$$u_{\text{thermal}}^2(T=0) = \frac{3\hbar^2}{4mk_B\Theta_D}.$$

The temperature-independent offset in addition to this zero-point motion, u_{static}^2 , when observed, can be a strong indication of the presence of static (non-thermal) disorder in a system. The temperature dependence of the u^2 parameters is described well by the Debye model as shown by the fits in Fig. 2. In Table I we summarize these fits. The u_{static}^2 parameters are negligibly small at all atomic sites, and the Debye temperatures are appropriate for the elements they represent.

Investigations of the local environment around the metal ions were performed using temperature dependent XAFS above the Tb L_{III} edge and the Ti K edge. XAFS oscillations occur above a core-level x-ray absorption edge, and are due to the interaction between the outgoing photoelectron from the absorbing atom and the component of this photoelectron that is back-scattered by neighboring atoms. The oscillations are periodic in the pair distance, r , and the photoelectron wave number, $k = \sqrt{2m(E - E_0)}/\hbar$, where E is the incident x-ray energy and E_0 is the energy at the absorption edge. XAFS analysis gives information about the radial distance distribution around the absorbing atomic species. In particular, pair distances, r_i , and pair-distance distribution widths, σ_i^2 , can be obtained for the first few atomic shells, i , out to about 5 Å. These XAFS data were analyzed using the UWXAFS package²⁸. First, the XAFS function $\chi = \mu/\mu_0 - 1$ is extracted after determining the atomic background absorption, μ_0 , obtained with the UWXAFS program AUTOBK by passing a cu-

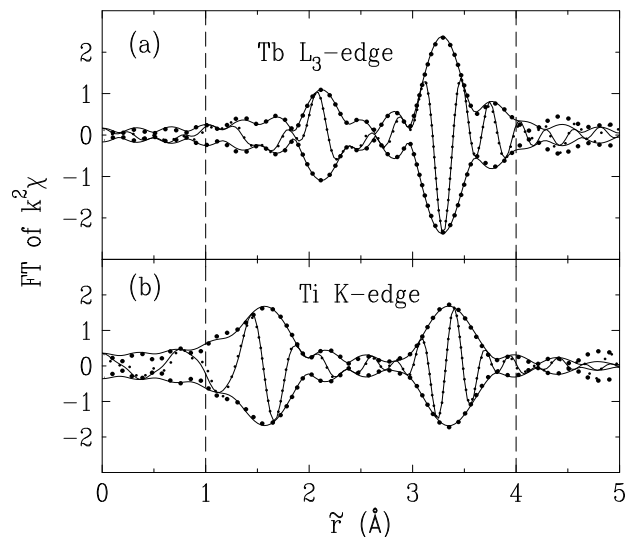


FIG. 4: Magnitude of the Fourier transformed (FT) XAFS data from Fig. 3 (thick-dotted lines) and the real part of the XAFS (thin-dotted lines) as function of distance from the probe atoms, (a) Tb L_3 -edge and (b) Ti K -edge. XAFS data in the range of 4.0 – 13.0 Å⁻¹ are used for the Fourier transform with a 0.5 Å⁻¹ wide Hanning window. Solid lines are the best fits and the vertical lines indicate the fit regions.

bic spline through the absorption data, μ . The k -space XAFS data for both measured edges are shown in Fig. 3. Multiple scans were obtained at each edge and temperature, with excellent reproducibility.

Figure 4 shows the magnitude and the real part of the Fourier transformed XAFS for both edges. Note that the peaks are shifted on the \tilde{r} axis from their true bond lengths due to the phase shift of the back-scattered photoelectron. This phase shift, as well as other details of the complex back-scattering function, differ for each atomic species, although they are well approximated by the theoretical treatment provided by the FEFF8 code.²⁹ Detailed fits are therefore necessary to obtain quantitative information. Solid lines show the best fit of a multiple shell model that assumes full occupancy of each of the sites, but allows the r_i and the σ_i^2 parameters for each shell to vary, with some exceptions. In particular, the Tb-Ti and Tb-Tb pairs near 3.60 Å are constrained to have the same pair distance, as are the Ti-Ti and Ti-Tb pair distances. The fit results are given in Table II and Fig. 5. Additional details of the XAFS analysis and the determination of the uncertainty of parameters have been given elsewhere.^{28,30}

The σ^2 data were analyzed analogously to the NPD u^2 parameters described above, except that a *correlated*-Debye model^{32,33} was used to account for correlated motion/displacements of the atom pairs. This model for σ^2 is the same as the Debye model (Eq. 1 and 2) except that a correlated-Debye temperature, Θ_{cD} , is used to differentiate from the regular Debye model, the reduced mass, μ , of the atom pairs is used, and the phonon density of

TABLE II: XAFS fit results at 20 K. The overall amplitude reduction factors, S_0^2 , were determined to be 0.96(9) for the Tb L_{III} -edge fits and 0.80(6) for the Ti K -edge fits. The number of fit parameters (10 and 13, respectively), is much less than the number of independent data points determined by Stern's rule³¹ (19 for each). N is the coordination number for the fully occupied model. Bond lengths of atomic pairs determined using XAFS (r) are compared to the NPD results (r_{NPD}) at 45 K. The correlated-Debye temperatures, Θ_{cD} , and the temperature-independent offsets, σ_{static}^2 , were determined by fitting with a correlated-Debye model^{32,33} over the measured temperature range (20-300 K). The correlation parameter ϕ is given by Eq. 4.

| Atomic pair | N | $r(\text{\AA})$ | $r_{\text{NPD}}(\text{\AA})$ | $\Theta_{\text{cD}}(\text{K})$ | $\sigma_{\text{static}}^2(\text{\AA}^2)$ | ϕ |
|--------------------|-----|-----------------|------------------------------|--------------------------------|--|----------|
| Tb-O(2) | 2 | 2.199(6) | 2.1939(6) | 875(170) | -0.0002(7) | 0.61(7) |
| Tb-O(1) | 6 | 2.490(9) | 2.4958(7) | 450(20) | 0.0004(5) | 0.18(7) |
| Tb-Ti ¹ | 6 | 3.598(6) | 3.583(1) | 300(20) | -0.0004(8) | 0.40(15) |
| Tb-Tb ¹ | 6 | 3.598(6) | 3.583(1) | 269(11) | -0.0003(3) | 0.65(9) |
| Ti-O(1) | 6 | 1.985(7) | 1.9699(5) | 600(50) | -0.0009(10) | 0.60(7) |
| Ti-Ti ² | 6 | 3.596(7) | 3.583(1) | 500(60) | -0.0005(7) | 0.55(8) |
| Ti-Tb ² | 6 | 3.596(7) | 3.583(1) | 300(15) | -0.0003(5) | 0.38(10) |

¹ Tb-Ti & Tb-Tb bond length constrained together

² Ti-Ti & Ti-Tb bond length constrained together

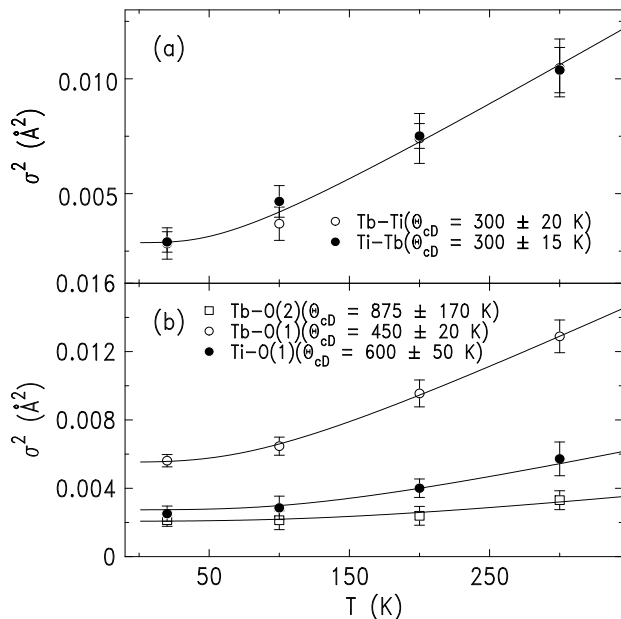


FIG. 5: Debye-Waller factor(σ^2) as a function of temperature. (a) Tb-Ti and Ti-Tb pairs, and (b) Tb-O(1), Tb-O(2) and Ti-O(1) pairs determined at Tb L_3 -edge and Ti K -edge. Solid lines are the best fits with the correlated-Debye model (see Table II). Ti-Ti pairs are omitted for clarity.

states for a given pair at distance R is given by

$$\rho = \frac{3\omega^2}{\omega_D^3} \left[1 - \frac{\sin(\omega R/c)}{\omega R/c} \right], \quad (3)$$

where ω_D is the usual Debye cut-off frequency and $c = \omega_D/k_D$. The Debye wave vector is given by $k_D = (6\pi^2/V)^{1/3}$, where V is the mean volume per atom in the material. The expression in brackets of Eq. 3 takes into account the correlated motion of the atom pair. This model fits the temperature dependence of the measured σ^2 's well (Fig. 5) with only negligible static displace-

ments, σ_{static}^2 's, as shown in Table II. This lack of pair-distance disorder agrees well with the lack of positional disorder determined from the NPD results above.

A Tb/Ti site interchange model was also considered for these XAFS data. However, XAFS is insensitive to such site interchange in this system because correlations in the fits between the (nominally same) Tb-Tb and Tb-Ti pair distances (as well as the Ti-Tb, Ti-Ti distances), their σ^2 's, and the alleged interchange render the results inconclusive.

IV. DISCUSSION

The primary result of the above measurements is that the $\text{Tb}_2\text{Ti}_2\text{O}_7$ lattice is extremely well ordered, both on average (NPD) and locally (XAFS). This result is supported by the high quality of the fits, the low estimated errors, and the temperature dependence of the mean-squared displacement parameters. These data thus strongly support the conclusion made by previous authors that $\text{Tb}_2\text{Ti}_2\text{O}_7$ is an excellent laboratory to study the effects of geometric frustration in the absence of lattice disorder.

The discrepancy between our results and those of van de Velde *et al.*²² must be attributable to either the different techniques used to measure the structure or to produce the sample. Since powder x-ray diffraction should be able to distinguish the cations, we must assume that the synthesis method used in van de Velde *et al.*, namely, preparing $\text{Tb}_2\text{Ti}_2\text{O}_7$ by the citrate method from $\text{TiO}(\text{OH})_2$ and a solution of Tb_4O_7 in nitric acid, results in an imperfect pyrochlore lattice. This situation is not inconceivable, since considerably lower temperatures and shorter times are used in this method compared to the solid state reaction method used here.¹⁵

Very recently, Lian *et al.*¹⁴ reported an x-ray diffraction study of the entire $\text{RE}_2\text{Ti}_2\text{O}_7$ (RE=rare-earth) series. Although they do not focus on $\text{Tb}_2\text{Ti}_2\text{O}_7$ or on

the detailed search for lattice disorder presented here, they report a room-temperature x parameter for the oxygen $48f$ site of 0.3281(5), which is consistent with our measurement of 0.3279(1), but not with the value of 0.317(2)³⁴ found by van de Velde *et al.*²² A value of $x \approx 0.328$ is, however, consistent with that found in the RE₂Ti₂O₇ series,¹⁴ while a value less than 0.32 is a gross deviation. As noted earlier, this parameter is very sensitive to lattice distortions, which could be due to antisite disorder, oxygen excess or deficiency, etc. In fact, Minervini *et al.*²³ find that the theoretical ideal value for x given no lattice disorder is ~ 0.3278 , in excellent agreement with our measurements and those of Lian *et al.* This agreement, together with the fact that Lian *et al.* used a flux-growth synthesis technique and obtained similar results to those presented here, is therefore consistent with our interpretation that the main reason van de Velde *et al.* found Tb₂Ti₂O₇ to be an imperfect pyrochlore is the synthesis method, not the measurement technique, nor is the disorder generic to the material itself.

There are a few interesting points to note about the measured structure and its vibrational properties. One is that the single-site Debye temperatures (from NPD) do not scale as expected in a Debye solid, that is, by the square root of the ratio of their masses. In this way, one sees that the Tb atomic vibrations are governed by much softer phonons than the Ti atoms [$\sqrt{m_{\text{Ti}}/m_{\text{Tb}}}\Theta_{\text{D}}(\text{Ti}) \approx 330$ K, while $\Theta_{\text{D}}(\text{Tb})=220$ K].

Another aspect to consider is the correlated displacements of the atom pairs. Since we have both neutron diffraction and XAFS measurements, we can extract the correlations by combining the results from both techniques. The instantaneous distance ($\Delta\vec{r}_{AB}$) between two atoms (A, B) is equal to the difference of the instantaneous displacements of the individual sites, $\Delta\vec{r}_A - \Delta\vec{r}_B$. Taking $\sigma_{AB}^2 = \langle \Delta\vec{r}_{AB}^2 \rangle$, $u_X^2 = \langle \Delta\vec{r}_X^2 \rangle$ and $u_A u_B \phi = \langle \Delta\vec{r}_A \cdot \Delta\vec{r}_B \rangle$, we then have

$$\sigma_{AB}^2 = u_A^2 + u_B^2 - 2\phi u_A u_B. \quad (4)$$

The correlation coefficient, ϕ , describes the motion or displacements of an atom relative to the other atom, taking the values +1 for two atoms moving together in the same direction, -1 for the atoms moving in fully opposite directions, and 0 for uncorrelated motion/displacements. The ϕ 's of Tb₂Ti₂O₇ at the lowest temperature extracted from the XAFS and diffraction measurements are summarized in Table II. The motions of the two O(2) oxygens located at ~ 2.2 Å from the Tb atom and the six O(1) oxygens located at ~ 2.0 Å from Ti atom are correlated in the motions to Tb and Ti, respectively, with ϕ of $\sim 60\%$. It is somewhat surprising that their motions are not more highly correlated with such short bond lengths, especially compared to, say, the copper-oxide superconductors.³⁵ More interestingly, the Tb-O(1) pairs are nearly uncorrelated in their motions, with a ϕ of only 0.2. Therefore, the motions of the O(1) atoms are governed mainly by the Ti sublattice, and not by the Tb sublattice. This result is consistent with the Tb sites exhibiting softer

phonons than expected from the Ti vibrations.

Given these vibrational properties, one should consider the charge distribution in the various ligands. One simple method is to determine whether the bond-valence sums³⁶ for the Tb and Ti oxygen environments correspond to the expected values of +3.0 and +4.0, respectively. Indeed, we obtain +3.01 and +3.95 from the NPD data, indicating that the charge is distributed as expected, given the measured coordination and bond lengths. Therefore, the measured lack of correlation between Tb and O(1) atoms and the soft Tb phonons are most likely a generic feature of a well-ordered pyrochlore lattice, such as Ti₂Mn₂O₇, or any of the other ferromagnetic pyrochlores.

A natural question to ask then is “Why is Tb₂Ti₂O₇ structurally so well ordered?” To this end, we can only speculate as to why, for instance, Y₂Mo₂O₇ exhibits distortions while Tb₂Ti₂O₇ does not. Ionic size arguments are marginally fruitful, since the ionic-size ratio³⁷ for Tb₂Ti₂O₇ ($r_A/r_B = 1.72$) is rather different than for Y₂Mo₂O₇ ($r_A/r_B = 1.57$). However, both of these values fall well within the range 1.46 to 1.80 typical of the pyrochlores.¹³ On the other hand, the negligibly small amount of static disorder on all atomic sites and between all near-neighbor pairs might suggest that the interaction of corner sharing spins is not strong enough to distort the atomic sites, as has been conjectured for Y₂Mo₂O₇.^{18,19} This explanation is supported by the relatively small Curie-Weiss temperature of ~ -19 K in Tb₂Ti₂O₇, compared to ~ -200 K in Y₂Mo₂O₇.³⁸

V. CONCLUSION

We have examined the bulk and local structure of the spin liquid pyrochlore Tb₂Ti₂O₇ by powder neutron diffraction and XAFS at the Tb L_{III} and Ti K edges. These data indicate a high degree of crystalline order, suggesting that this compound forms a perfect pyrochlore lattice with no intersite mixing or anion disorder. Furthermore, analysis of the temperature dependence of the atomic displacement parameters and mean-squared displacements shows that the static lattice disorder is negligible. Analysis of the Debye temperatures and the correlations between various site displacements show that, vibrationally, the Tb and Ti sublattices are partially decoupled, and that the more plentiful O(1) atoms are more tightly bound to the Ti sites. This compound, with its near absence of local and bulk structural disorder and antiferromagnetic nearest-neighbor interactions,^{15,38} is therefore an appropriate system to study the elusive 3-dimensional, low-temperature, spin liquid.

Acknowledgments

It is a pleasure to acknowledge A. Cull and I. Swainson for their assistance with the experiments at Chalk River, and S. Short for her assistance with the experiments

at the Intense Pulsed Neutron Source (IPNS). Work at Lawrence Berkeley National Laboratory was supported by the Director, Office of Science, U.S. Department of Energy (DOE) under Contract No. DE-AC03-76SF00098. Work at Brookhaven National Laboratory was supported by the Division of Material Sciences, DOE, under contract DE-AC02-98CH10886. Neutron diffraction data

were collected at the Chalk River Laboratories NRU reactor and at the IPNS, which is funded by the DOE, Office of Basic Energy Sciences (OBES), Materials Sciences, under Contract W-31-109-Eng-38. X-ray absorption data were collected at the Stanford Synchrotron Radiation Laboratory, a national user facility operated by Stanford University for the DOE, OBES.

-
- * Present address: Chonbuk National University, Jeonju, 561-756, Korea; Electronic address: swghan@mail.chonbuk.ac.kr
- † Electronic address: jason.gardner@nist.gov
- ‡ Electronic address: chbooth@lbl.gov
- ¹ B. D. Gaulin, *Magnetic Systems with Competing Interactions* (World Scientific, Singapore, 1994).
 - ² A. P. Ramirez, *Handbook on Magnetic Materials* (Elsevier, Amsterdam, 2001), vol. 13, chap. 4, p. 423.
 - ³ *Highly Frustrated Magnetism 2000 Conference Proceedings* (Can. J. Phys., vol. 79, Waterloo, Canada, 2001).
 - ⁴ J. N. Reimers, A. J. Berlinsky, and A. C. Shi, Phys. Rev. B **43**, 865 (1991).
 - ⁵ B. C. den Hertog and M. J. P. Gingras, Phys. Rev. Lett. **84**, 3430 (2000).
 - ⁶ M. Enjarlran, M. J. P. Gingras, Y.-J. Kao, A. Del Maestro, and H. R. Molavian, J. Phys.: Condens. Matter (in press), cond-mat/0308092.
 - ⁷ S. F. Edwards and P. W. Anderson, J. Phys. F: Metal Phys. **5**, 965 (1975).
 - ⁸ B. Canals and C. Lacroix, Phys. Rev. Lett. **80**, 2933 (1998).
 - ⁹ S.-H. Lee, C. Broholm, M. F. Collins, L. Heller, A. P. Ramirez, Ch. Kloc, E. Bucher, R. W. Erwin, and N. Lacey, Phys. Rev. B **56**, 8091 (1997).
 - ¹⁰ P. Schiffer, A. P. Ramirez, K. N. Franklin, and S.-W. Cheong, Phys. Rev. Lett. **77**, 2085 (1996).
 - ¹¹ N. P. Raju, E. Gmelin, and R. K. Kremer, Phys. Rev. B **46**, 5405 (1992).
 - ¹² O. A. Petrenko, C. Ritter, M. Yethiraj, and D. McK Paul, Phys. Rev. Lett. **80**, 4570 (1998).
 - ¹³ M. A. Subramanian, G. Aravamudan, and G. V. Subba Rao, Prog. Solid State Chem. **15**, 55 (1983).
 - ¹⁴ J. Lian, J. Chen, L. M. Wang, R. C. Ewing, J. M. Farmer, L. A. Boatner, and K. B. Helean, Phys. Rev. B **68**, 134107 (2003), the values reported in Fig. 2 of this work for the 48*f* positional parameter, x , from Ref. 23 are in error by about -0.004.³⁹ Please see Ref. 23 for this information.
 - ¹⁵ J. S. Gardner, B. D. Gaulin, S.-H. Lee, C. Broholm, N. P. Raju, and J. E. Greedan, Phys. Rev. Lett. **83**, 211 (1999).
 - ¹⁶ M. J. P. Gingras, B. C. den Hertog, M. Faucher, J. S. Gardner, S. R. Dunsiger, L. J. Chang, B. D. Gaulin, N. P. Raju, and J. E. Greedan, Phys. Rev. B **62**, 6496 (2000).
 - ¹⁷ J. S. Gardner, B. D. Gaulin, A. J. Berlinsky, P. Waldron, S. R. Dunsiger, N. P. Raju, and J. E. Greedan, Phys. Rev. B **64**, 224416 (2001).
 - ¹⁸ C. H. Booth, J. S. Gardner, G. H. Kwei, R. H. Heffner, F. Bridges, and M. A. Subramanian, Phys. Rev. B **62**, R755 (2000).
 - ¹⁹ A. Keren and J. S. Gardner, Phys. Rev. Lett. **87**, 177201 (2001).
 - ²⁰ B. D. Gaulin, J. N. Reimers, T. E. Mason, J. E. Greedan, and Z. Tun, Phys. Rev. Lett. **69**, 3244 (1992).
 - ²¹ L. H. Brixner, Inorg. Chem. **3**, 1065 (1964).
 - ²² G. M. H. van de Velde, B. C. Lippens, S. J. Korf, and J. Boeijmsma, Powder Diffraction **5**, 229 (1990).
 - ²³ L. Minervini, R. W. Grimes, Y. Tabira, R. L. Withers, and K. E. Sickafus, Philos. Mag. A **82**, 123 (2002).
 - ²⁴ A. C. Larson and R. B. Von Dreele, *General Structure Analysis System, Los Alamos National Laboratory Report No. LAUR 86-748* (2000).
 - ²⁵ J. N. Reimers, J. E. Greedan, and M. Sato, J. Solid State Chem. **72**, 390 (1988).
 - ²⁶ S. X. Wang, B. D. Begg, L. M. Wang, R. C. Ewing, W. J. Weber, and K. V. G. Hutton, J. Mater. Res. **14**, 4470 (1999).
 - ²⁷ A. Chartier, C. Meis, W. J. Weber, and L. R. Corrales, Phys. Rev. B **65**, 134116 (2002).
 - ²⁸ E. A. Stern, M. Newville, B. Ravel, Y. Yacoby, and D. Haskel, Physica B **208** & **209**, 117 (1995), find further information of UWXAFS at <http://depts.washington.edu/uwxafs>.
 - ²⁹ A. L. Ankudinov, B. Ravel, J. J. Rehr, and S. D. Conradson, Phys. Rev. B **58**, 7565 (1998).
 - ³⁰ S.-W. Han, E. A. Stern, D. Haskel, and A. R. Moodenbaugh, Phys. Rev. B **66**, 094101 (2002).
 - ³¹ E. A. Stern, M. Qian, Y. Yacoby, S. M. Heald, and H. Maeda, Physica C **209**, 331 (1993).
 - ³² G. B. Beni and P. M. Platzman, Phys. Rev. B **14**, 1514 (1976).
 - ³³ E. D. Crozier, J. J. Rehr, and R. Ingalls, in *X-Ray Absorption: Principles, Applications, Techniques of EXAFS, SEXAFS, XANES*, edited by D. Konigsberger and R. Prins (Wiley, New York, 1988), p. 373.
 - ³⁴ Some diffraction studies of pyrochlore structures place the *A* atoms on the 16*c* site and the *B* atoms on the 16*d* site, in contrast to the present work. In this case, the x -parameter for the 48*f* sites is related by taking $0.75-x$. Also, the O(2) atoms are then on the 8*a* sites while the 8*b* sites are vacant, rather than the other way around.
 - ³⁵ C. H. Booth, F. Bridges, J. B. Boyce, T. Claeson, B. M. Lairson, R. Liang, and D. A. Bonn, Phys. Rev. B **54**, 9542 (1996).
 - ³⁶ I. D. Brown and D. Altermatt, Acta Cryst. **B41**, 244 (1985).
 - ³⁷ R. D. Shannon, Acta Crystallogr. A **32**, 7519 (1976).
 - ³⁸ M. J. P. Gingras, C. V. Stager, N. P. Raju, B. D. Gaulin, and J. E. Greedan, Phys. Rev. Lett. **78**, 947 (1997).
 - ³⁹ R. W. Grimes, private communication.